Using legacy core material to assess subsurface carbon storage reservoir potentiality

Ryan L. Payton[1]*, Domenico Chiarella[1] and Andrew Kingdon[2]

[1]Clastic Sedimentology Investigation (CSI), Department of Earth Sciences, Royal Holloway, University of London, Egham, Surrey TW20 0EX, UK

[2]British Geological Survey, Keyworth, Nottingham NG12 5GG, UK

RLP, 0000-0001-5724-0695; DC, 0000-0003-2482-0081; AK, 0000-0003-4979-588X

*Correspondence: ryan.payton.2015@live.rhul.ac.uk

Abstract: The growing importance of subsurface carbon storage for tackling carbon emissions requires an accurate characterization of potential reservoirs to understand their capabilities. In this context, the use of legacy data originally acquired in the last fifty years for scientific projects and petroleum exploration and production activities would represent a suitable cost-effective solution and help to maximize the value of this extended national asset. Core material represents the only direct observation of subsurface deposits and must be preserved from the current disposal process related to the decommissioning of hydrocarbon fields. In this contribution, a suite of samples from core material stored at national (i.e. British Geological Survey) and local (i.e. Department of Earth Sciences, Royal Holloway, University of London) core repositories, previously characterized at the micro scale using X-ray micro-computed tomographic (μCT) imaging are discussed. Using this technique, it has been possible to investigate how pore and grain geometries control crucial features of a suitable reservoir such as porosity and permeability. The aim of this contribution is to describe the methodology behind digital image analysis (DIA) following μCT imaging applied to core material. We show how DIA can be used to provide significant measures of reservoir suitability when making initial assessments of storage reservoirs, without the need for expensive and time-consuming analyses.

Carbon capture, utilization and storage (CCUS) is a technology which has been used in various forms since the 1970s (Hill *et al.* 2013; Núñez-López and Moskal 2019). At this time CO_2 was used as an injectant for enhanced oil recovery (EOR), undoubtedly trapping CO_2 in the subsurface in the process without this being the primary aim and without consideration for trapping security. In 1996 the first geological carbon storage (GCS) pilot study at the Sleipner CO_2 storage site (offshore Norway) began storing CO_2 (Equinor 2019), with the added aim of ensuring that the carbon remained in the subsurface for a geologically significant period of time. Since this initial landmark project, many additional pilot projects have been launched as well as a handful of full-scale storage facilities. As of October 2021 there were 135 large-scale carbon capture and storage (CCS) facilities at various stages between early development and full operation (27 of the 135) with 71 of these projects being added in 2021 (Global CCS Institute 2021*a*).

A recent shift in society's perception of climate change and CCUS has resulted in an influx of public funding both directly and indirectly benefiting CCUS. Indirect support includes the introduction of carbon tax credits, rewarding emitters for storing CO_2 or utilizing it for other purposes, such as in the USA through the 45Q tax credits scheme expansion (IEA 2020). Direct support has come in the form of funding promises such as €10 bn up to 2030 from the European Union Innovation Fund (Page *et al.* 2019), $12.5 bn from the Infrastructure Investment and Jobs Act in the USA (Global CCS Institute 2021*b*), $1.8 bn from the Norwegian government for the Longship project (IEA 2020) and £1 bn from the UK government as part of the Carbon Capture and Storage Infrastructure Fund (CIF) (Government of the United Kingdom 2021). The advent of increased funds being made available for CCS comes with the need to make the best possible use of them to deliver positive results, thereby encouraging further funding. This can, in part, be achieved by carrying out cost-effective and valuable initial site screening.

To make the best decisions when selecting a site for geological carbon storage, a number of static factors can be outlined which characterize a possibly successful subsurface storage site. (1) The storage reservoir must contain a suitable amount of space for satisfying the CO_2 storage needs specified for the given project. This is likely to be determined primarily by reservoir porosity (Bachu *et al.* 2007; Bradshaw *et al.* 2007; Pingping *et al.* 2009), but is also influenced by the relationship between the strength of the cap rock and injection rate. (2) There must be suitable conditions for injected fluids

From: Neal, A., Ashton, M., Williams, L. S., Dee, S. J., Dodd, T. J. H. and Marshall, J. D. (eds) 2023. *Core Values: the Role of Core in Twenty-first Century Reservoir Characterization*. Geological Society, London, Special Publications, **527**, 387–397. First published online November 29, 2022, https://doi.org/10.1144/SP527-2022-18

to move through the reservoir unit in order to make the injection process straightforward and to allow the available volume of the reservoir to be accessed. This may be investigated through measurements of permeability and connected porosity (Raza *et al.* 2017; Cui *et al.* 2018; Hoteit *et al.* 2019). (3) The site must possess suitable mechanisms of ensuring that CO_2 remains contained in the subsurface. This is typically investigated through permeability and mechanical analysis of the caprock or seal overlying the reservoir alongside detection and structural analyses of fractures and faults (Shipton *et al.* 2004; Dockrill and Shipton 2010; Bond *et al.* 2017). Finally, (4) ideally the reservoir unit should possess favourable mineralogy, fluid chemistry and pressure and temperature conditions to facilitate reactions with the injected CO_2 to produce stable carbon-bearing precipitates. Such precipitates include calcite, siderite and magnesite (Zhang *et al.* 2015; Zhang and DePaolo 2017). Each of these four broad criteria for a suitable GCS reservoir may be investigated initially using legacy core material, prior to a thorough site-specific assessment.

Rock drilling techniques and coring can be dated back to *c.* 3000 BC in ancient Egypt (Gorelick and Gwinnett 1983). Since then, coring has proven a useful technique to acquire rock samples for many different purposes. The first known oil wells were drilled in China in AD 347 (Ulrich Vogel 1993) and drilling is an activity still used today to assess the subsurface or extract resources. In this process, the acquisition of core material is important to obtain direct observations and analyses of the stratigraphy and to eventually assess source, seal and reservoir potentiality. Since 1968, over 15 500 individual wells have been spudded for oil and gas exploration, appraisal or production on the United Kingdom Continental Shelf (UKCS). Of these, some 8000 have been partially cored with a total of over 350 km of core and 4.5 million samples of cuttings being acquired. Some 15 000 onshore UK wells have been cored, including over 400 of the 22 200 onshore oil and gas exploration and production wells. Samples from each borehole drilled for the hydrocarbon industry including a representative volume, typically one-third, of every core collected are stored at the National Geoscience Data Centre, co-located with the British Geological Survey to support research for national public good (Fig. 1). Considering the high costs for acquiring a core section, they represent a great asset, a valuable resource and a powerful tool for contributing to the future decarbonization process. Unfortunately, high costs related to operators' storage facilities are pushing hydrocarbon companies to dispose of their portion of collected legacy cores, typically two-thirds of each cored length, that are no longer of any interest for their activities.

Fig. 1. Photograph of a small portion of the core material stored within the National Geoscience Data Centre at the British Geological Survey (BGS) core store. Source: British Geological Survey © UKRI. BGS photo ID P900669 available from BGS Geoscenic.

Core materials are fundamental for assessing reservoir properties. The use of digital rock physics (DRP) to measure porosity and permeability is becoming increasingly popular (Van Geet *et al.* 2003; Blunt *et al.* 2013; Jarzyna *et al.* 2016; Thomson *et al.* 2020*b*; Payton *et al.* 2021). To assess the potentiality of a stratigraphic interval as a CO_2 storage reservoir it is critical to determine whether there is enough storage capacity, and that injected CO_2 will be able to effectively move through the formation. This, therefore, implies that successful GCS projects occur in highly porous and permeable reservoirs, such as the Utsira Formation at the Sleipner site (Zweigel *et al.* 2004).

The aim of this short contribution is to present an established digital methodology and the consequent results of reservoir characterization analysis of subsurface intervals using μCT (X-ray micro-computed tomography) images of core material. The objective is to increase awareness of the value of legacy core material for the phase of energy transition.

Methodology

Preparing, imaging and processing core samples and measuring their features using μCT and digital image analysis is a process which has been recently documented in detail (Thomson *et al.* 2018, 2019, 2020*a*, *b*; Payton *et al.* 2021, 2022). Here we provide a synthesis of each step in digital sample analysis based upon the work undertaken by the aforementioned authors.

Sample preparation

Plugs of core material are extracted from regions of interest in the main core to acquire a smaller volume of material to work with. These are typically *c.* 2 cm

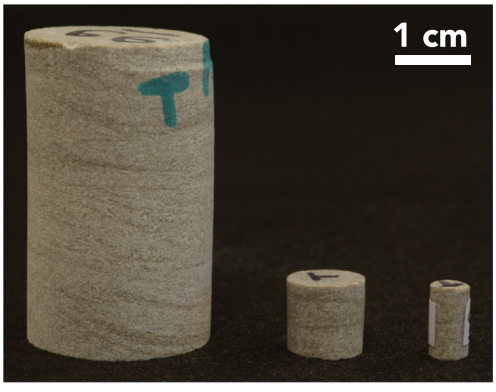

Fig. 2. Sandstone plugs extracted from geological core. The largest plug is initially cut from the original core run before being cut into smaller plugs. The smallest plug is used for micro-computed tomography (μCT) imaging. 'T' in green and black marker indicates the top of the samples.

in diameter and up to 10 cm long, depending on core volume retained (Fig. 2). From this volume a smaller mini-plug is required to be extracted for use in a μCT scanner, depending on the individual scanner and the desired field of view. For the samples presented in this work (Thomson *et al.* 2020*b*; Payton *et al.* 2021) a Zeiss Xradia Versa 520 scanner was used at the London Natural History Museum, for which a mini-plug *c.* 5 mm in diameter and 10 mm in length was suitable. The cylindrical shape of the sample to be imaged is important as the imaging process acquires a stack of circular fields of view, therefore, a cylinder is the most efficient geometry to scan (Ketcham and Carlson 2001). This also has the added benefit of the X-ray beam achieving equal penetration throughout the scanning process, resulting in the reduction of image artefacts (Ketcham and Carlson 2001).

Preparation of the mini-plug(s) from the core plug (Fig. 2) can pose several challenges depending on the friability of the material being sampled. Sampling of especially friable material is impossible as the core degrades during the sampling process. Payton *et al.* (2021) found it necessary to use an epoxy resin to consolidate plugs of sandstone prior to cutting mini-plugs. Injection of resin is usually apparent when interrogating the resulting tomographic images, manifesting as dark-rimmed spherical objects. Despite the difference in density between air and resin, these two phases appear as very similar dark shades of grey in geological tomographic images, causing no difficulty in phase segmentation as both are considered as pore space (Payton *et al.* 2021).

Due to the small size of the mini-plug typically required for scanning, it is most effective to produce mini-plugs by hand grinding and shaping core material. Conventional cutting equipment is typically too large and lacks the level of control required to produce such small pieces of material.

Imaging

The process of acquiring μCT images is fundamentally based upon density differences between material phases, resulting in variable amounts of X-ray attenuation. Denser materials are able to attenuate more X-rays, and so appear brighter in the tomograms as opposed to less dense materials which attenuate less X-rays, and so appear darker (Fig. 3). Each material possesses an X-ray attenuation coefficient which varies with the X-ray energy employed by the scanner. The greater the difference between these values, the more easily distinguished the associated phases are in the greyscale tomograms.

When imaging sandstone samples the importance of considering the attenuation coefficients of phases other than quartz is negligible in many cases. However, if the goal of imaging is to differentiate between many phases, such as igneous minerals, then it may be necessary to identify an optimum X-ray energy to produce the greatest phase contrast possible. For further information about the linear attenuation coefficient and how this varies in different materials we refer the reader to Ketcham and Carlson (2001), Hanna and Ketcham (2017) and Bam *et al.* (2020).

The level of detail which can be acquired in the output images is dependent on the CT scanner itself as well as the chosen field of view. For sandstone materials it has been shown that a voxel resolution of *c.* 3 μm^3 provides a suitable level of detail for accurately studying the geometry of the pore microstructures and grains (Thomson *et al.* 2018, 2020*a*, *b*; Payton *et al.* 2021, 2022). Greater resolutions may be achieved by focusing on a smaller area of the mini-plug, using more powerful techniques

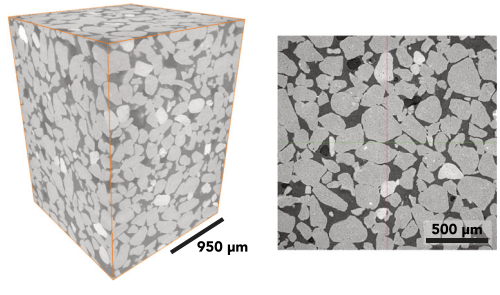

Fig. 3. Micro-computed tomography (μCT) 3D volume rendering (left) and individual image slice (right). Images have been filtered to remove noise. Darker regions show pore spaces whilst paler regions are solid material.

such as synchrotron tomography or by increasing the X-ray energy used. However, this can lead to issues with overall image quality and artefacts.

Processing

In almost all cases a level of image processing, post-acquisition is beneficial to making accurate measurements on any acquired CT images. The goal of pre-processing is to increase the signal to noise ratio across the images. A variety of artefacts may be present as a result of the scanning process including beam-hardening, ring artefacts and general image noise (Ketcham and Carlson 2001; Cnudde and Boone 2013; Hanna and Ketcham 2017). Most digital image processing software packages provide tools specifically designed to clean up the image data, removing or lessening artefacts and noise. It is often the case that one tool or algorithm alone is not entirely effective and instead a combination of filters is required (Fig. 4). It is important to consider how much processing is required to reach a set goal for use of the images. Processing is effectively changing the raw data artificially. Therefore, over-processing may change the data significantly, causing features to be lost or gained which are artificial.

Payton *et al.* (2021) and Thomson *et al.* (2020*b*) perform 3D volume cropping of the raw image reconstruction prior to filtering. Cropping allows the removal of outer voxels not belonging to the sample but also trimming of the extremities of the mini-plug volume. This is where beam-hardening is most extreme and may not always be resolved to a suitable degree by image filters.

The non-local means (NLM) filter is a popular and very effective tool in removing most of the salt and pepper noise throughout the image stack (Buades *et al.* 2008; Thomson *et al.* 2018; Garfi *et al.* 2020) and is an effective starting step (Fig. 4). Further tweaking of the NLM filter parameters may be required or additional filters such as mean, median, Gaussian or anisotropic diffusion to suitably clean the image for the intended purpose. For example, Payton *et al.* (2021) and Thomson *et al.* (2020*b*) find that a NLM filter alone is suitable for basic phase identification and measurements of porosity and permeability. However, Payton *et al.* (2022) show that addition of a median filter allows for more effective grain boundary segmentation (Fig. 4).

Measurements

After processing CT images to maximize their quality, the process of making measurements of features and properties can begin. The next step in acquiring useful data from images is to segment the individual phases from one another (Fig. 5). Segmentation is the process by which image voxels are labelled according to the phase to which they belong. This process is carried out either automatically using algorithms (Otsu 1979; Payton *et al.* 2021) or manually by selecting peaks on a histogram of greyscale values (Thomson *et al.* 2020*b*; Payton *et al.* 2021). Both techniques work by using a greyscale histogram, representative of the X-ray attenuation coefficient measured in each voxel across the sample volume. Depending on how successful filtering has been and the variety of materials in a sample an automatic or manual approach may be appropriate (Payton *et al.* 2021).

Having separated individual phases a variety of measurements can be made:

(1) Porosity – the fraction of voxels labelled as void space can be calculated and therefore represents total porosity in the material (Fig. 5). A connectivity algorithm can be applied to determine which voxels belonging to the void space facilitate entire connectivity throughout the study volume (Fig. 6). Measuring the fraction of these connected voxels, therefore, provides

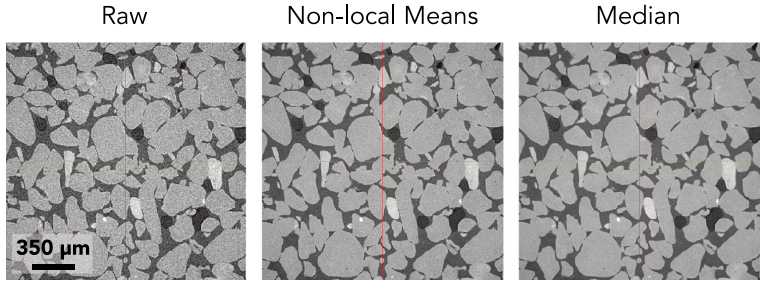

Fig. 4. Examples of the effect of image filtering on micro-computed tomography (µCT) image slices. The raw image is covered with salt and pepper noise making segmentation difficult. The non-local means filter removes the majority of the noise, improving the phase contrast and signal to noise ratio. The addition of a median filter has a smoothing effect and removes most of the blemishes remaining on the granular phase, improving the definition of grain boundaries.

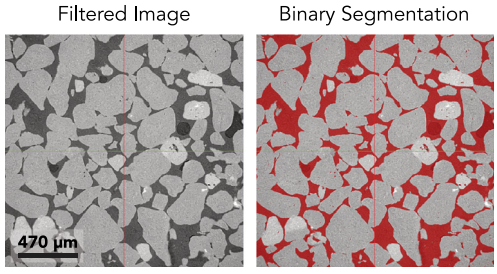

Fig. 5. Example of binary segmentation of the pore space. The red areas have been segmented and labelled to belong to the pore space phase. Comparison can be made with the original image to show the quality of the segmentation.

a value of connected porosity. The accuracy of porosity measurements made using this technique are reliant on the voxel size of the 3D reconstructed volume. Porosity below the resolving capability of the scanner is omitted and therefore measurements must be considered to represent macro porosity at this scale rather than true porosity. Despite this, acceptable representative measurements may be acquired, as highlighted by the close agreement between µCT DIA porosity measurements and those of bulk porosity from a well logging tool by Payton *et al.* (2021).

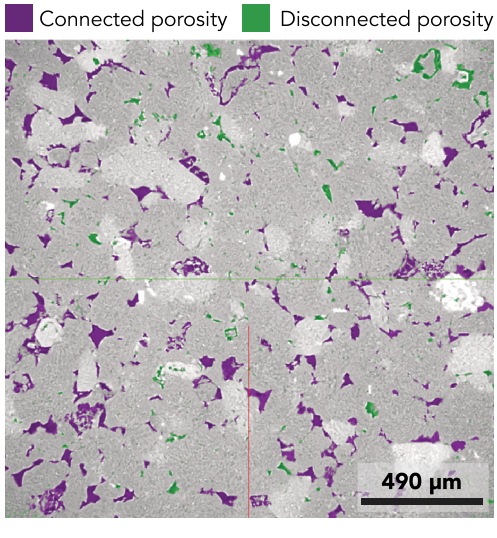

Fig. 6. Segmentation of both the connected (purple) and disconnected (green) porosity. First, the total porosity is segmented, a connectivity algorithm is then used to determine the voxels of the porosity phase which facilitate connectivity throughout the sample in 3D.

(2) Permeability – the connected pore network of voxels can be used as a 3D domain to run a numerical simulation to calculate permeability. This is performed using the 'absolute permeability experiment simulation' tool in the commercial software package PerGeos. This tool is based on solving the Stokes equations using the finite volume method to obtain a velocity and pressure field which can be used with the Darcy flow equation to determine a value of permeability (Thomson *et al.* 2020*b*; Payton *et al.* 2021). When employing the 'absolute permeability experiment simulation' tool, a value of 10^{-6} has been found to be the most effective tolerance value for the convergence of the simulation solution (Thomson *et al.* 2019), allowing for comparable measurements to be made between studies. A variety of tools exist to perform this type of simulation and measurement (Bultreys *et al.* 2015; Gostick *et al.* 2016; Payton *et al.* 2021), of which many are based on a similar approach. Permeability may also be determined through digital image analysis using pore network models (PNMs) more rapidly but typically with an acceptable but lower accuracy (Varloteaux *et al.* 2013). Measurements of permeability using this approach may be limited in their accuracy in cases where pore-lining phases, which inhibit fluid flow, are present. Phases such as illite, kaolinite and chlorite may be indistinguishable from the bulk of the granular material due to scanning resolution or greyscale contrast and therefore, their detrimental impact on permeability cannot be considered in the permeability simulation process. Consequently, permeability measurements made using a µCT DIA/DRP approach must be assumed to be upper extremes for given study samples.

(3) Pore and throat geometries – a pore network model (PNM) is an effective technique for making measurements of pore and throat diameter, throat radius and pore coordination number. PNMs approximate a pore structure through using balls as pores and connected sticks as throats (Youssef *et al.* 2007; Raoof *et al.* 2013), shown in Figure 7. Despite their apparent simplicity, they show close agreement with measurements made using direct methods which are more computationally expensive (Varloteaux *et al.* 2013). PNMs are generated using a series of algorithms which are effectively described by Youssef *et al.* (2007) and Thomson *et al.* (2018, 2019). Briefly, a skeletonization algorithm generates a one-voxel-thick skeleton through

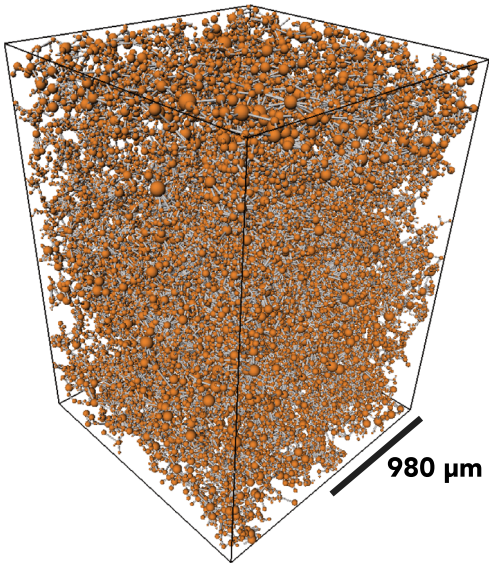

Fig. 7. Example of a pore network model. Pores are represented by orange spheres which are scaled to the pore diameter. Throats which connect the pores are represented by grey pipes which are uniformly scaled in this case.

the centre of the pore structure. Thresholds are defined where junctions form in the skeleton to identify dead ends, pore lines or throat lines. The classification as pore or throat depends on the ratio of line length and maximum radius. If the largest possible radius of a line is greater than its length it is assigned as a pore, otherwise as a throat (Payton *et al.* 2021). The ball and stick model can then be interrogated to make measurements of pore and throat geometries.

(4) Grain analysis – typical grain measurements such as size, sphericity and sorting can be acquired through implementation of a watershed segmentation algorithm (Shi and Yan 2015; Beucher and Meyer 2018; Kong and Fonseca 2018; Sun *et al.* 2019; Leonti *et al.* 2020). Thomson *et al.* (2020*a*) demonstrate how digital image analysis can be applied to separate individual grains in CT images. Payton *et al.* (2022) refine the technique by including an additional filter to facilitate more accurate grain segmentation. Having segmented grains into individual features, they may be labelled and interrogated individually to acquire the aforementioned grain properties. We refer the reader to Payton *et al.* (2022) for more details on this process.

Case studies

The following sections present examples of legacy onshore and offshore core material sampled and analysed in the Royal Holloway, University of London Earth Sciences Department in recent years using the described digital image analysis technique on µCT images and the key results.

Wilmslow Sandstone Formation, Sellafield BH13B, Cumbria, UK (onshore)

Payton *et al.* (2021) apply a µCT-based approach to carrying out a porosity and permeability analysis of the Wilmslow Sandstone Formation (WSF). Using this technique, they identify a range of porosities between 9.77 and 26.4% and are able to determine that across the seven study samples the bulk majority of porosity was in fact connected. Payton *et al.* (2021) attempt to quantify the error in their porosity measurements through the difference in automatic and manual segmentation with the largest deviation being an error of $\pm 2.58\%$. The authors used wireline log measurements of neutron and bulk porosity to validate their digital image analysis measurements of porosity, for which they found a good level of agreement (Payton *et al.* 2021).

As a result of the significant connectivity identified, permeability experiment simulations returned a range of results from 40 to 6040 mD. Consequently, the authors were able to recommend further investigation of this study site for use as a GCS reservoir based on a preliminary pore-scale assessment.

Pore network modelling and 3D volume rendering observations of connected and disconnected porosity identified the presence of significant disconnected intragranular porosity (Payton *et al.* 2021). It was found that the pore size distributions indicated a significant number of very small pores which were identified as predominantly intragranular. The difference in mean pore radius between total and connected porosity highlighted the importance of larger pores in contributing to connectivity. In contrast, samples with similar mean pore radii between both types of porosity showed significant intergranular disconnected porosity.

The WSF material was also used alongside µCT images of the Brae Formation sandstone to determine the upper percolation threshold or crossover threshold (Payton *et al.* 2021). The upper percolation threshold is the amount of porosity required within a given sample to establish a fully connected network of porosity. Below this threshold, porosity is partially connected and above this threshold, fully connected. Using the digitally acquired total and connected porosity measurements they determined the upper percolation threshold to be *c.* 10%,

defining the regime transition from partial connectivity to full connectivity.

Scottish Middle Coal Measures Formation, UKGEOS GGC01, Glasgow, UK (onshore)

Sandstone from the Scottish Middle Coal Measures Formation (SMCMF) was also studied by Payton *et al.* (2021). They carried out a porosity analysis, determining there to be between 0.04 and 1.65% porosity present in the four study samples. Connectivity analysis revealed no connectivity within the pore structures and, consequently, no permeability. Due to the minimal amount of porosity in the samples the authors noted that automatic segmentation was unsuitable and instead manual segmentation was necessary.

μCT imaging was combined with optical microscopy to identify the cause of such minimal porosity. Optical microscopy allowed clear identification of significant amounts of cement, infilling the pore network (Payton *et al.* 2021). Following this, the 3D μCT image volume reconstructions allowed for spatial investigation of the cement phase. The greater image resolution allowed for investigation into the contact between the cement and grain phases to determine whether any localized regions of porosity were present (Payton *et al.* 2021).

Minard Formation, Porcupine Basin, North Atlantic (offshore)

Twelve samples from the Minard Formation (MF) sandstone in the Porcupine Basin were imaged and analysed in terms of porosity and permeability and their grains (Payton *et al.* 2022). A porosity range of 9–20.4% was identified with all samples exhibiting varying degrees of connectivity, resulting in permeability measurements of up to 1070 mD.

Following the work presented by Thomson *et al.* (2020*a*), implementation of a watershed segmentation algorithm was used to identify and measure individual 3D grains (Payton *et al.* 2022). This allowed for identification of a positive relationship between grain sphericity and both porosity and permeability. Payton *et al.* (2022) found no relationship between grain size and porosity or permeability. They used the measures of shape and size to constrain a Kozeny–Carman type porosity–permeability relationship, finding that inclusion of grain parameters in a fit equation was less effective than a simple fit based upon porosity alone. Ultimately, using the automated technique to acquire large numbers of rapid grain measurements from μCT images, they determine that a simpler fit of the form $K = 10^{5.54}\ \phi^{3.7}$ provides a better porosity–permeability fit owing to the Kozeny–Carman assumption that grains are spherical. Consequently, they recommend further investigation into developing a model capable of incorporating non-spherical grains.

Otter Sandstone Formation, English Channel, UK (offshore)

Thirty samples from the Otter Sandstone Formation (OSF) were used alongside the previously described case study sample suites to determine a robust value for the upper percolation threshold as well as adding further constraint to a porosity–permeability relationship determined from digital measurements.

These samples display a porosity range of 0.4–17.6%, spanning the range that lacked data points following analysis of the WSF, SMCMF and MF sandstone. Permeability was found to range from 0 to 4655 mD as a result of varying degrees of connectivity in the samples. Combination of all described case study suites results in a well-characterized total-connected porosity relationship. An upper percolation threshold or crossover threshold was able to be identified at *c.* 14%, better constrained than the result previously reported by Payton *et al.* (2021).

Using all of the study sample suites a better-defined porosity–permeability relationship could be defined according to $K = 10^{5.68}\ \phi^{3.88}$. Additionally, using the large volume of data from the OSF, the relative influence of pores and throats on connectivity could be investigated. A significant offset between data points of total porosity and connected porosity when measuring mean coordination number and pore radius is present. No such offset is present in measurements of mean throat length and radius, indicating that the pores are most influential in facilitating connectivity.

Brae Formation sandstone, North Sea, UK (offshore)

Whilst Payton *et al.* (2021, 2022) use measurements from images of the Brae Formation sandstone (BFS) to supplement the analysis of the previously described case study suites, Thomson *et al.* (2020*b*) investigate the porosity–permeability relationship alongside the upper and lower percolation thresholds and microporosity. They report a connected macroporosity range of 0–15.2% in their eight BFS samples; however, they identify and segment an additional microporous phase in their CT images. Microporosity contributed a further 2.6–10.7% porosity throughout the sample suite, facilitating permeability measurements of up to 795 mD. μCT imaging allowed Thomson *et al.* (2020*b*) to investigate the spatial occurrence of this microporous phase which is of importance for facilitating greater connectivity and permeability within the

BFS material. They were able to tie microporosity occurrence to sites where secondary and accessory minerals accumulate, such as clay, lithic fragments and muscovite using CT images in conjunction with scanning electron microscopy (SEM) imaging.

In order to quantify the impact of regions of microporosity, Thomson *et al.* (2020*b*) performed two sets of image segmentation and analyses. They segmented the apparent microporous regions as solid grain phase in one case and as void space in another. This allowed identification of an upper and lower limit of porosity and permeability when considering the microporous phase. Unfortunately, the imaging capabilities of μCT were unable to suitably resolve the microporous regions clearly enough to produce more accurate measurements. Supplementary imaging using techniques such as FIB-SEM (focused ion beam scanning electron microscopy) would be required to gain even further understanding of the pore network in these particular samples.

Similarly to Payton *et al.* (2021), Thomson *et al.* (2020*b*) use digital image analysis to determine the percolation threshold in sandstone. The authors use BFS samples alongside others (Thomson *et al.* 2019) to estimate an upper percolation threshold of *c.* 10%. They also find that their sample suite allows for identification of a lower percolation threshold of *c.* 5%. Consequently, they are able to define boundaries for regime changes from isolated to partially effective to fully effective porosity.

Finally, Thomson *et al.* (2020*a*) use digital image analysis of μCT images of BFS samples to investigate the grains, further developed by Payton *et al.* (2022). Thomson *et al.* (2020*a*) identify no clear relationship between the grain characteristics and porosity or permeability but are able to make rapid measurements using many data points of sorting, skewness and grain size in their samples.

Concluding remarks and future outlook

It is undeniable that CCUS projects are required alongside other low carbon technologies in order for the global community to reach the required Net-Zero targets. CCUS provides a method of not only reducing emissions by capturing them before they reach the atmosphere but also conceivably of progress towards going carbon negative. CCUS also allows particularly difficult to abate technologies, such as steel, cement and fertilizer production, to effectively reduce their carbon emissions. As confidence grows in CCUS and it becomes more economically viable more reservoirs will be sought for use.

Delivering the predicted uptake in CCUS will require identification of many storage reservoirs worldwide. The need to minimize both the technical and economic risks associated with this technology means that initial screening assessments will likely focus on those geological formations that are already well characterized. Therefore, those that have significant volumes of legacy core material available will be desirable owing to the ability to use the material for testing appropriate stratigraphic units. Whilst an abundance of legacy wells in a carbon storage site can cause challenges with regards to storage integrity (Zhang and Bachu 2011), legacy material remains a valuable asset for conducting initial site screening prior to incorporation of additional datasets to make further decisions. The significant cost of drilling and core extraction, especially on continental shelf areas, which are typically carried out by oil and gas companies, makes legacy core a highly valuable resource. As hydrocarbon exploration is predicted to decrease significantly as society pursues low carbon alternatives, it is likely that far less new core will become available. Maximizing the value of the existing core archive, therefore, will become imperative.

In this work we have described how small volumes of legacy core material can be used, with success, in providing initial characterization and assessment of potential CCUS reservoirs. A key advantage of digital rock physics (DRP) and digital image analysis (DIA) techniques is that they are non-destructive, thereby retaining the value of the legacy core material. This also allows for repeat digital experiments to be made easily on the same sample volumes. Furthermore, digital imaging of legacy core material facilitates the sharing of physical representations of geological samples through platforms such as the Digital Rocks Portal more readily than would be possible with actual physical samples. Such image repositories allow workflows to be streamlined on a given core sample as multiple instances of a digital physical representation can be worked on in parallel.

DRP and DIA techniques together provide non-destructive analytical capabilities for initial reservoir characterization of porosity, permeability and mineralogy, three key areas of carbon storage site screening and assessment. The added ability of these techniques to investigate parameters such as pore and grain shape and size, which influence the dynamic behaviour of fluids at the pore scale, adds further value. The fact that this approach requires only small volumes of material highlights the value of both these technologies and legacy core material itself. Despite this, some limitations of this approach remain, such as image resolution and pore-lining phase distinction for making highly accurate porosity and permeability measurements. This highlights that whilst this approach is valuable for initial screening and assessment of potential storage sites, it will remain essential for additional datasets and

techniques to be applied alongside μCT DIA to make further decisions.

We foresee a continued uptake in the use of DIA and DRP within Earth Sciences, especially in the field of CCUS using legacy core material, owing to the wealth of information and data that can be acquired. Other new areas of research, including extracting geothermal heat and storage of energy in the form of heat or compressed air in aquifers, will also require similar reservoir characterization. Consequently, the quality and capability of the tools and techniques being developed to add further value to μCT digital image datasets will only continue to increase. Furthermore, active work on reliable upscaling of micro-scale measurements for representative rock volumes has the potential to provide even greater insight from μCT digital image datasets to CCUS reservoir assessment beyond the initial phase. Approaches to this challenge include fractal-scaling (Munawar *et al.* 2021), a combined Darcy–Brinkman–Stokes approach (Menke *et al.* 2021), pore network model stitching (Kohanpur and Valocchi 2020), correlation with whole core imaging (Hertel *et al.* 2018) and percolation theory (Liu and Regenauer-Lieb 2011). Legacy core material is vital to this process and should be exploited for the readily available information it can provide on possible carbon storage reservoirs as CCUS grows in the near future.

Acknowledgements The authors gratefully acknowledge the assistance of Simon Harris (British Geological Survey) from the NGDC in preparing this manuscript and Dan Condon (British Geological Survey) for carrying out the British Geological Survey internal review. We acknowledge the work of Kevin D'Souza (Royal Holloway, University of London) in photographing core material. Additionally, we acknowledge Brett Clark (Natural Histroy Museum, London) for his support and guidance in μCT imaging. This manuscript was published with the permission of the Executive Director of the British Geological Survey. Samples and data are derived from the UK Geoenergy Observatories Programme funded by the UKRI Natural Environment Research Council and delivered by the British Geological Survey.

Competing interests The authors declare that they have no known competing financial interests or personal relationships that could have appeared to influence the work reported in this paper.

Author contributions **RLP**: conceptualization (equal), funding acquisition (equal), writing – original draft (lead), writing – review & editing (equal); **DC**: conceptualization (equal), project administration (lead), supervision (lead), writing – original draft (supporting), writing – review & editing (equal); **AK**: supervision (supporting), writing – original draft (equal), writing – review & editing (equal).

Funding RLP and DC acknowledge support from a NERC DTP studentship (grant number NE/L002485/1) as well as further financial support through a CASE partnership with the British Geological Survey as part of their British University Funding Initiative. AK acknowledges support from the British Geological Survey via NERC national capability.

Data availability Data sharing is not applicable to this article as no datasets were generated or analysed during the current study.

References

Bachu, S., Bonijoly, D., Bradshaw, J., Burruss, R., Holloway, S., Christensen, N.P. and Mathiassen, O.M. 2007. CO_2 storage capacity estimation: methodology and gaps. *International Journal of Greenhouse Gas Control*, **1**, 430–443, https://doi.org/10.1016/S1750-5836(07)00086-2

Bam, L.C., Miller, J.A. and Becker, M. 2020. A mineral X-ray linear attenuation coefficient tool (MXLAC) to assess mineralogical differentiation for X-ray computed tomography scanning. *Minerals*, **10**, 8–11, https://doi.org/10.3390/min10050441

Beucher, S. and Meyer, F. 2018. The morphological approach to segmentation: the watershed transformation. *In*: Thompson, B.J. and Dougherty, E. (eds) *Mathematical Morphology in Image Processing*, CRC Press, 433–481, https://doi.org/10.1201/9781482277234-12

Blunt, M.J., Bijeljic, B. *et al*. 2013. Pore-scale imaging and modelling. *Advances in Water Resources*, **51**, 197–216, https://doi.org/10.1016/J.ADVWATRES.2012.03.003

Bond, C.E., Kremer, Y. *et al*. 2017. The physical characteristics of a CO_2 seeping fault: the implications of fracture permeability for carbon capture and storage integrity. *International Journal of Greenhouse Gas Control*, **61**, 49–60, https://doi.org/10.1016/J.IJGGC.2017.01.015

Bradshaw, J., Bachu, S., Bonijoly, D., Burruss, R., Holloway, S., Christensen, N.P. and Mathiassen, O.M. 2007. CO_2 storage capacity estimation: issues and development of standards. *International Journal of Greenhouse Gas Control*, **1**, 62–68, https://doi.org/10.1016/S1750-5836(07)00027-8

Buades, A., Coll, B. and Morel, J.-M. 2008. Nonlocal image and movie denoising. *International Journal of Computer Vision*, **76**, 123–139, https://doi.org/10.1007/s11263-007-0052-1

Bultreys, T., Van Hoorebeke, L. and Cnudde, V. 2015. Multi-scale, micro-computed tomography-based pore network models to simulate drainage in heterogeneous rocks. *Advances in Water Resources*, **78**, 36–49, https://doi.org/10.1016/J.ADVWATRES.2015.02.003

Cnudde, V. and Boone, M.N. 2013. High-resolution X-ray computed tomography in geosciences: a review of the current technology and applications. *Earth-Science*

Reviews, **123**, 1–17, https://doi.org/10.1016/j.earscirev.2013.04.003

Cui, G., Wang, Y., Rui, Z., Chen, B., Ren, S. and Zhang, L. 2018. Assessing the combined influence of fluid-rock interactions on reservoir properties and injectivity during CO_2 storage in saline aquifers. *Energy*, **155**, 281–296, https://doi.org/10.1016/j.energy.2018.05.024

Dockrill, B. and Shipton, Z.K. 2010. Structural controls on leakage from a natural CO_2 geologic storage site: Central Utah, USA. *Journal of Structural Geology*, **32**, 1768–1782, https://doi.org/10.1016/J.JSG.2010.01.007

Equinor 2019. Sleipner partnership releases CO_2 storage data, https://www.equinor.com/en/news/2019-06-12-sleipner-co2-storage-data.html

Garfi, G., John, C.M., Berg, S. and Krevor, S. 2020. The sensitivity of estimates of multiphase fluid and solid properties of porous rocks to image processing. *Transport in Porous Media*, **131**, 985–1005, https://doi.org/10.1007/s11242-019-01374-z

Global CCS Institute 2021*a*. *Global Status of CCS 2021*, https://www.globalccsinstitute.com/wp-content/uploads/2021/10/2021-Global-Status-of-CCS-Report_Global_CCS_Institute.pdf

Global CCS Institute 2021*b*. US Congress Passes Bill with the Single Largest CCS Infrastructure Investment Ever – Global CCS Institute, https://www.globalccsinstitute.com/news-media/latest-news/us-congress-passes-bill-with-the-single-largest-ccs-infrastructure-investment-ever/

Gorelick, L. and Gwinnett, J.A. 1983. Ancient Egyptian stone-drilling. *Expedition Magazine – Penn Museum*.

Gostick, J., Aghighi, M. *et al*. 2016. OpenPNM: a pore network modeling package. *Computing in Science & Engineering*, **18**, 60–74, https://doi.org/10.1109/MCSE.2016.49

Government of the United Kingdom 2021. The Carbon Capture and Storage Infrastructure Fund: an update on its design, https://www.gov.uk/government/publications/design-of-the-carbon-capture-and-storage-ccs-infrastructure-fund/the-carbon-capture-and-storage-infrastructure-fund-an-update-on-its-design-accessible-webpage

Hanna, R.D. and Ketcham, R.A. 2017. X-ray computed tomography of planetary materials: a primer and review of recent studies. *Geochemistry*, **77**, 547–572, https://doi.org/10.1016/j.chemer.2017.01.006

Hertel, S.A., Rydzy, M., Anger, B., Berg, S., Appel, M. and de Jong, H. 2018. Upscaling of digital rock porosities by correlation with whole-core CT-scan histograms. *Petrophysics*, **59**, 694–702, https://doi.org/10.30632/PJV59N5-2018a8

Hill, B., Hovorka, S. and Melzer, S. 2013. Geologic carbon storage through enhanced oil recovery. *Energy Procedia*, **37**, 6808–6830, https://doi.org/10.1016/j.egypro.2013.06.614

Hoteit, H., Fahs, M. and Soltanian, M.R. 2019. Assessment of CO_2 injectivity during sequestration in depleted gas reservoirs. *Geosciences*, **9**, 199, https://doi.org/10.3390/geosciences9050199

IEA 2020. *Energy Technology Perspectives 2020 – Special Report on Carbon Capture Utilisation and Storage*, https://doi.org/10.1787/208b66f4-en

Jarzyna, J.A., Krakowska, P.I. *et al*. 2016. X-ray computed microtomography – a useful tool for petrophysical properties determination. *Computational Geosciences*, **20**, 1155–1167, https://doi.org/10.1007/s10596-016-9582-3

Ketcham, R.A. and Carlson, W.D. 2001. Acquisition, optimization and interpretation of X-ray computed tomographic imagery: applications to the geosciences. *Computers & Geosciences*, **27**, 381–400, https://doi.org/10.1016/S0098-3004(00)00116-3

Kohanpur, A.H. and Valocchi, A.J. 2020. Pore-network stitching method: a pore-to-core upscaling approach for multiphase flow. *Transport in Porous Media*, **135**, 659–685, https://doi.org/10.1007/s11242-020-01491-0

Kong, D. and Fonseca, J. 2018. Quantification of the morphology of shelly carbonate sands using 3D images. *Géotechnique*, **68**, 249–261, https://doi.org/10.1680/jgeot.16.P.278

Leonti, A., Fonseca, J. *et al*. 2020. Optimized 3D segmentation algorithm for shelly sand images. Proceedings of the *6th World Congress on Electrical Engineering and Computer Systems and Science*. CIST 107, https://doi.org/10.11159/cist20.107

Liu, J. and Regenauer-Lieb, K. 2011. Application of percolation theory to microtomography of structured media: percolation threshold, critical exponents, and upscaling. *Physical Review E*, **83**, 16106, https://doi.org/10.1103/PhysRevE.83.016106

Menke, H.P., Maes, J. and Geiger, S. 2021. Upscaling the porosity–permeability relationship of a microporous carbonate for Darcy-scale flow with machine learning. *Scientific Reports*, **11**, 2625, https://doi.org/10.1038/s41598-021-82029-2

Munawar, M.J., Vega, S., Lin, C., Alsuwaidi, M., Ahsan, N. and Bhakta, R.R. 2021. Upscaling reservoir rock porosity by fractal dimension using three-dimensional micro-computed tomography and two-dimensional scanning electron microscope images. *Journal of Energy Resources Technology, Transactions of the ASME*, **143**, https://doi.org/10.1115/1.4047589/1084712

Núñez-López, V. and Moskal, E. 2019. Potential of CO_2-EOR for near-term decarbonization. *Frontiers in Climate*, **1**, 5, https://doi.org/10.3389/fclim.2019.00005

Otsu, N. 1979. A threshold selection method from gray-level histograms. *IEEE Transactions on Systems, Man, and Cybernetics*, **9**, 62–66, https://doi.org/10.1109/TSMC.1979.4310076

Page, B., Turan, G. *et al*. 2019. *Global Status of CCS 2019*, https://www.globalccsinstitute.com/wp-content/uploads/2019/12/GCC_GLOBAL_STATUS_REPORT_2019.pdf

Payton, R.L., Fellgett, M., Clark, B.L., Chiarella, D., Kingdon, A. and Hier-Majumder, S. 2021. Pore-scale assessment of subsurface carbon storage potential: implications for the UK Geoenergy Observatories project. *Petroleum Geoscience*, **27**, https://doi.org/10.1144/petgeo2020-092

Payton, R.L., Chiarella, D. and Kingdon, A. 2022. The influence of grain shape and size on the relationship between porosity and permeability in sandstone: a digital approach. *Scientific Reports*, **12**, 7531, https://doi.org/10.1038/s41598-022-11365-8

Pingping, S., Xinwei, L. and Qiujie, L. 2009. Methodology for estimation of CO_2 storage capacity in reservoirs. *Petroleum Exploration and Development*, **36**, 216–220, https://doi.org/10.1016/S1876-3804(09)60121-X

Raoof, A., Nick, H.M., Hassanizadeh, S.M. and Spiers, C.J. 2013. PoreFlow: a complex pore-network model for simulation of reactive transport in variably saturated porous media. *Computers & Geosciences*, **61**, 160–174, https://doi.org/10.1016/J.CAGEO.2013.08.005

Raza, A., Gholami, R., Rezaee, R., Bing, C.H., Nagarajan, R. and Hamid, M.A. 2017. Preliminary assessment of CO_2 injectivity in carbonate storage sites. *Petroleum*, **3**, 144–154, https://doi.org/10.1016/j.petlm.2016.11.008

Shi, Y. and Yan, W.M. 2015. Segmentation of irregular porous particles of various sizes from X-ray microfocus computer tomography images using a novel adaptive watershed approach. *Géotechnique Letters*, **5**, 299–305, https://doi.org/10.1680/jgele.15.00100

Shipton, Z.K., Evans, J.P., Kirschner, D., Kolesar, P.T., Williams, A.P. and Heath, J. 2004. Analysis of CO_2 leakage through 'low-permeability' faults from natural reservoirs in the Colorado Plateau, east-central Utah. *Geological Society, London, Special Publications*, **233**, 43–58, https://doi.org/10.1144/GSL.SP.2004.233.01.05

Sun, Q., Zheng, J. and Li, C. 2019. Improved watershed analysis for segmenting contacting particles of coarse granular soils in volumetric images. *Powder Technology*, **356**, 295–303, https://doi.org/10.1016/j.powtec.2019.08.028

Thomson, P.-R., Aituar-Zhakupova, A. and Hier-Majumder, S. 2018. Image segmentation and analysis of pore network geometry in two natural sandstones. *Frontiers in Earth Science*, **6**, 1–14, https://doi.org/10.3389/feart.2018.00058

Thomson, P.-R., Hazel, A. and Hier-Majumder, S. 2019. The influence of microporous cements on the pore network geometry of natural sedimentary rocks. *Frontiers in Earth Science*, **7**, 48, https://doi.org/10.3389/feart.2019.00048

Thomson, P.-R., Ellis, R., Chiarella, D. and Hier-Majumder, S. 2020*a*. Microstructural analysis from X-ray CT images of the Brae Formation Sandstone, North Sea. *Frontiers in Earth Science*, **8**, 246, https://doi.org/10.3389/feart.2020.00246

Thomson, P.-R., Jefferd, M., Clark, B.L., Chiarella, D., Mitchell, T.M. and Hier-Majumder, S. 2020*b*. Pore network analysis of Brae Formation sandstone, North Sea. *Marine and Petroleum Geology*, **122**, 104614, https://doi.org/10.1016/J.MARPETGEO.2020.104614

Ulrich Vogel, H. 1993. The Great Well of China. *Scientific American*, **268**, 116–121, https://doi.org/10.1038/scientificamerican0693-116

Van Geet, M., Lagrou, D. and Swennen, R. 2003. Porosity measurements of sedimentary rocks by means of microfocus X-ray computed tomography (μCT). *Geological Society, London, Special Publications*, **215**, 51–60, https://doi.org/10.1144/GSL.SP.2003.215.01.05

Varloteaux, C., Vu, M.T., Békri, S. and Adler, P.M. 2013. Reactive transport in porous media: pore-network model approach compared to pore-scale model. *Physical Review E*, **87**, 23010, https://doi.org/10.1103/PhysRevE.87.023010

Youssef, S., Rosenberg, E., Gland, N.F., Kenter, J.A., Skalinski, M. and Vizika, O. 2007. High Resolution CT and pore-network models to assess petrophysical properties of homogeneous and heterogeneous carbonates. *SPE/EAGE Reservoir Characterization and Simulation Conference*, 28–31 October 2007, Abu Dhabi, UAE, 280–291, https://doi.org/10.2118/111427-MS

Zhang, M. and Bachu, S. 2011. Review of integrity of existing wells in relation to CO_2 geological storage: what do we know? *International Journal of Greenhouse Gas Control*, **5**, 826–840, https://doi.org/10.1016/j.ijggc.2010.11.006

Zhang, S. and DePaolo, D.J. 2017. Rates of CO_2 mineralization in geological carbon storage. *Accounts of Chemical Research*, **50**, 2075–2084, https://doi.org/10.1021/acs.accounts.7b00334

Zhang, S., DePaolo, D.J., Voltolini, M. and Kneafsey, T. 2015. CO_2 mineralization in volcanogenic sandstones: geochemical characterization of the Etchegoin Formation, San Joaquin Basin. *Greenhouse Gases: Science and Technology*, **5**, 622–644, https://doi.org/10.1002/ghg.1508

Zweigel, P., Arts, R., Lothe, A.E. and Lindeberg, E.B.G. 2004. Reservoir geology of the Utsira Formation at the first industrial-scale underground CO_2 storage site (Sleipner area, North Sea). *Geological Society, London, Special Publications*, **233**, 165–180, https://doi.org/10.1144/GSL.SP.2004.233.01.11